Biofabrication

PAPER

Multiscale hierarchical bioresorbable scaffolds for the regeneration of tendons and ligaments

Alberto Sensini[1], **Chiara Gualandi**[2,3], **Maria Letizia Focarete**[2,3,7], **Juri Belcari**[1], **Andrea Zucchelli**[1], **Liam Boyle**[4], **Gwendolen C Reilly**[5], **Alexander P Kao**[6], **Gianluca Tozzi**[6] and **Luca Cristofolini**[1,3,7]

[1] Department of Industrial Engineering, Alma Mater Studiorum—Università di Bologna, I-40131, Bologna, Italy
[2] Department of Chemistry 'G. Ciamician' and National Consortium of Materials Science and Technology (INSTM, Bologna RU), Alma Mater Studiorum—Università di Bologna, I-40126, Bologna, Italy
[3] Health Sciences and Technologies—Interdepartmental Center for Industrial Research (HST-ICIR), Alma Mater Studiorum—Università di Bologna, I-40064, Ozzano dell'Emilia, Bologna, Italy
[4] Department of Materials Science and Engineering, University of Sheffield, Sheffield S31 3JD, United Kingdom
[5] INSIGNEO Institute for in silico Medicine, University of Sheffield, Sheffield S31 3JD, United Kingdom
[6] School of Engineering, University of Portsmouth, Portsmouth PO1 3DJ, United Kingdom
[7] Authors to whom any correspondence should be addressed.

E-mail: luca.cristofolini@unibo.it **and** marialetizia.focarete@unibo.it

Keywords: tissue engineering, tendon and ligament tissue, electrospinning, multiscale hierarchical scaffolds, multiscale assembly

Supplementary material for this article is available online

OPEN ACCESS

RECEIVED
16 October 2018

REVISED
18 April 2019

ACCEPTED FOR PUBLICATION
9 May 2019

PUBLISHED
12 June 2019

Abstract

Lesions of tendons and ligaments account for over 40% of the musculoskeletal lesions. Surgical techniques and materials for repair and regeneration are currently not satisfactory. The high rate of post-operative complications and failures mainly relates to the technical difficulties in replicating the complex multiscale hierarchical structure and the mechanical properties of the native tendons and ligaments. With the aim of overcoming the limitations of non-biomimetic devices, we developed a hierarchical structure replicating the organization of tendons and ligaments. The scaffold consists of multiple bundles made of resorbable electrospun nanofibers of Poly-L-Lactic acid (PLLA) having tailored dimensions, wrapped in a sheath of nanofibers able to compact the construct. The bundles in turn consist of electrospun nanofibers with a preferential direction. High-resolution x-ray tomographic investigation at nanometer resolution confirmed that the morphology of the single bundles and of the entire scaffold replicated the hierarchical arrangement in the natural tendons and ligaments. To confirm that these structures could adequately restore tendons and ligaments, we measured the tensile stiffness, strength and toughness. The mechanical properties were in the range required to replace and repair tendons and ligaments. Furthermore, human fibroblasts were able to attach to the scaffolds and showed an increase in cell number, indicated by an increase in metabolic activity over time. Fibroblasts were preferentially aligned along the electrospun nanofibers. These encouraging *in vitro* results open the way for the next steps towards *in vivo* regeneration of tendons and ligaments.

1. Introduction

Tendon and ligament reconstruction presents a challenging clinical problem in orthopedics. In the United States, about 45% of the 32.8 million musculoskeletal injuries each year involve tendons and ligaments [1–3]. However, because current clinical techniques are unable to restore the complex hierarchical structure of the tendon and ligament and their excellent mechanical properties [4–6], post-operative complications and failures are common [7–9]. Furthermore, at the site of the lesion or fracture, scar tissue created after healing from the surgical treatment, may create morphological discontinuities which impair the mechanical properties and functionality [10]. The research field of tissue engineering aims to provide tools that enable reconstruction of these tissues using resorbable scaffolds. Different techniques are used to

produce scaffolds [6, 8, 9, 11, 12], but probably the most promising for tendon and ligament regeneration or substitution is electrospinning [13, 14]. Due to its ability to produce fibers of both natural and synthetic polymers with nanometric diameters, electrospinning has the potential to produce scaffolds morphologically very similar to the hierarchical structure of the tendon and ligament collagen fascicles and fibrils [4–6, 14–16]. Specific arrangement of the electrospinning setup allows alignment of the nanofibers in desired directions.

Researchers have approached tendon and ligament regeneration using electrospinning either by using singular units or building hierarchical multiscale assemblies [11–14, 17, 18]. Focusing on singular units, electrospun bundles and yarns [19, 20] are the scaffolds which can better mimic the morphological structure and mechanical properties of tendon and ligament fascicles. For example, Bosworth *et al* demonstrated that electrospun yarns obtained twisting electrospun mats of different resorbable materials, provided the required mechanical properties and cell proliferation [21–23]. Xu *et al* produced Poly (L-Lactide-*co*-ε-Caprolactone)/Collagen nanoyarns for tendon regeneration, by twisting nanofibers in a water vortex collector [24]. Pauly *et al* produced promising bundles of Poly (ε-Caprolactone) (PCL) for ligament regeneration, by wrapping portions of electrospun mats on a drum collector [25]. In a similar way, Sensini *et al* produced bundles of Poly-L-Lactic acid (PLLA) and Collagen crosslinked blends with mechanical properties of the same order of magnitude as human tendon fascicles in terms of Young Modulus (103.2 ±16.8 MPa) and failure stress (18.8 ± 3.8 MPa) [26]. An increases in number of human fibroblasts over time was observed [26]. Banik *et al* developed an electrospun scaffold of a high number of PCL nanofibers with a 'Chinese-finger trap' configuration, mainly composed of nanofibers axially aligned between two cylindrical ground collectors [27]. These approaches allow production of nanofibers similar to collagen fibrils, and with adequate composition, but the proposed constructs did not provide adequate strength and stiffness to replace or regenerate a tendon or ligament.

The alternative approach uses hierarchical assemblies that aim to reproduce the multiscale structure of a complete tendon or ligament, and provide adequate strength by joining several bundles or yarns in different configurations [11, 13, 17, 18]. Xu *et al* produced a multiscale scaffold by twisting yarns with encouraging mechanical properties and cell proliferation [24, 28]. Several approaches which involved twisting yarns of nanofibers have been tested using polydioxanone [29] and PCL/Chitosan blends reinforced with cellulose nanocrystals [30] to replace tendons and ligaments.

Assembling multiple bundles or yarns is certainly a promising approach to mimic the hierarchical structure of tendons and ligaments, but adequate mechanical strength and stiffness are achieved only if the bundles or yarns are densely arranged, otherwise significant cavities and a critical reduction of structural properties results. Therefore, a key point is to include in the multiscale production a method for compacting the bundles and yarns together. The outer surface of natural tendons and ligaments is wrapped in a epitenon/epiligament sheath [4–6]. Replicating this natural morphology would allow compaction of the bundles/yarns inside the scaffold, and higher mechanical properties. In conjunction an ideal sheath should be engineered so as to permit to cells to cross it, or at least to allow to biological fluids to bring the nutrients to the cells inside the scaffold structure. For example, Zhou *et al* electrospun a Poly(ethylene oxide) coating on a group of aligned monofilaments of Polyamide which were twisted during the coating [31]. Naghashzargar *et al* coated yarns of monofilaments of silk with PCL and P3HB, for possible tendon and ligament regeneration [32]. Padmakumar *et al* coated electrospun yarns of PLLA with an electrospun sheath of Poly (lactic-*co*-glycolic) acid fibers loaded with drugs, as a suture wire [33]. Recently Li *et al* produced an electrospun scaffold for nerve conduit, made of a coating of Poly (L-lactide-*co*-caprolactone) on electrospun yarns of PLLA, and studied the cell proliferation and ability to cross the membrane [34].

While promising steps have been taken both in the production of single bundles and yarns, and in possible methods for assembling a hierarchical structure, none of the developed solutions was able to mimic the hierarchical structure of tendons and ligaments, and at the same time, to provide adequate mechanical properties.

We report here a bottom-up method to produce an innovative multiscale hierarchical electrospun nanofibrous scaffold able to mimic both the hierarchical structure and the biomechanical properties of a tendon or a ligament. Several fascicle-inspired PLLA bundles were produced and grouped together by an electrospun PLLA sheath, similar to the epitenon-epiligament membrane, reproducing a whole tendon/ligament-like scaffold. With this method, we were able to manufacture resorbable scaffolds with suitable morphology, mechanical properties and cell growth to regenerate tendons and ligaments.

2. Materials and methods

2.1. Materials

Poly-L-lactic acid (PLLA) (Lacea H.100-E, $M_w = 8.4 \times 10^4$ g mol^{-1}, PDI = 1.7) was purchased from Mitsui Fine Chemicals (Dusseldorf, Germany). Dichloromethane (DCM) and Dimethylformamide (DMF) were purchased from Sigma-Aldrich (Sigma-Aldrich, Saint Louis, USA) and used as received. The following polymeric solution was prepared for

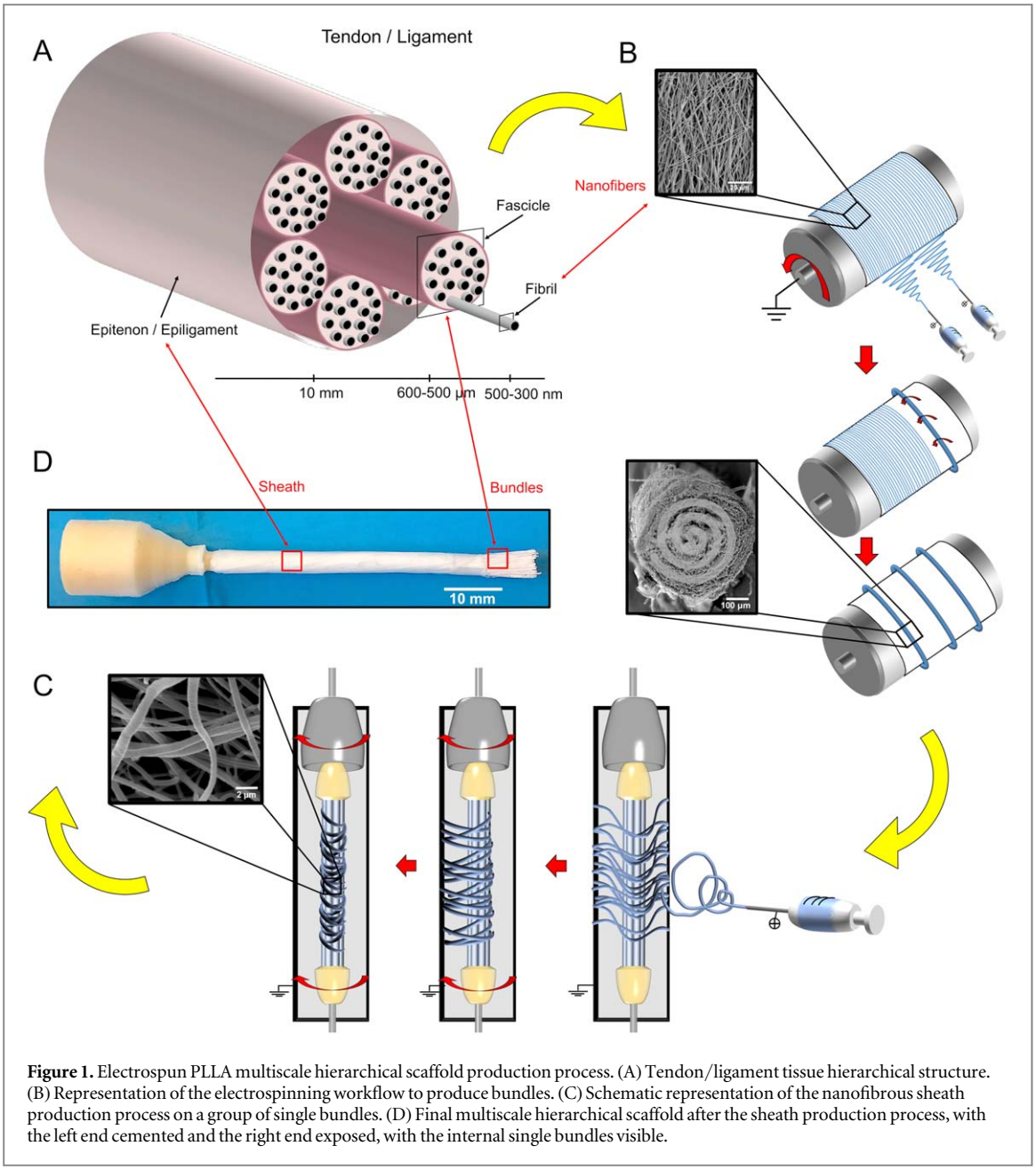

Figure 1. Electrospun PLLA multiscale hierarchical scaffold production process. (A) Tendon/ligament tissue hierarchical structure. (B) Representation of the electrospinning workflow to produce bundles. (C) Schematic representation of the nanofibrous sheath production process on a group of single bundles. (D) Final multiscale hierarchical scaffold after the sheath production process, with the left end cemented and the right end exposed, with the internal single bundles visible.

electrospinning: 13% (w/v) solution of PLLA dissolved in DCM:DMF = 65:35 (v/v).

To embed the extremities of the PLLA multiscale hierarchical scaffolds for the mechanical tests, an acrylic cement (Restray, Salmoiraghi Mulazzano, Italy), was used. For the hydration of both the PLLA single bundles and multiscale hierarchical scaffolds before the mechanical tests, 0.9% NaCl solution, purchased by S.A.L.F. (Cenate Sotto, Italy), was used.

2.2. Electrospinning and assembling the PLLA multiscale hierarchical scaffold

In this work, the complete hierarchical structure of a tendon or ligament (figure 1(A)) was reproduced by using two different electrospinning set-ups: a commercial electrospinning unit (Spinbow srl, Bologna, Italy) (figure S1(A) is available online at stacks.iop.org/BF/11/035026/mmedia) was employed to produce PLLA single bundles while a custom-made electrospinning apparatus was used to produce the sheath wrapping the multiscale hierarchical scaffold. Electrospinning was performed at room temperature and relative humidity 30%–40%. The commercial electrospinning unit is equipped with a linear sliding spinneret with two syringes configuration (40 mm apart), and a rotating drum collector. To control the flux of the solution, a syringe pump (KD Scientific 200 series, Illinois, USA) and two glass syringes containing the polymer solution and connected to two stainless-steel blunt-ended needles through two Teflon tubes, were used. The sliding spinneret with the two needles had a linear excursion of 120 mm along the collector,

with a speed of 1500 mm min^{-1}. PLLA solution was electrospun by applying the following processing conditions: applied voltage = 18 kV, feed rate = 1.2 ml h^{-1}, needles inner diameter = 0.84 mm, electrospinning time = 1 h. A rotating aluminum collector (length = 405 mm, diameter = 150 mm) turning at 2900 rpm (resulting in a peripheral speed of 22.8 m s^{-1}) was used to produce mats made of fibers preferentially aligned in the direction of drum rotation. The rotating collector was positioned 200 mm away from the tip needles. To reduce the risk of attachment and allow easy detachment of the mats from the drum, the collector was covered with a sheet of paper with a polyethylene layer (Turconi S.p.A, Ceriano Laghetto, Italy) following a consolidated procedure [26]. To obtain the PLLA single bundles, the mat was cut in rectangular strips and manually wrapped along the collector (figure 1(B)). To remove the PLLA single bundles from the collector, they were incised axially with a cutter. Thus, the final single bundles were as long as the circumference of the rotating collector (approximately 471 mm), and were made of fibers predominantly axially aligned. The bundles obtained with this process had a diameter of 550–600 μm.

To produce the PLLA multiscale hierarchical scaffold, the single bundles were cut into segments with a length of 100 mm each. To obtain a multiscale hierarchical scaffold with a mean diameter of 6.5 mm, 100 bundles were used. The extremities were tied together at first with Parafilm (Pechiney Plastic Packaging, Chicago, USA) and then were covered with paper tape. After this operation, a PLLA sheath of nanofibers was electrospun on the group of bundles for 3 h. To electrospin the sheath, a custom-made electrospinning apparatus was used, consisting of a high-voltage power supply (FuG Elektronik GmbH, Schechen, Germany) and a syringe pump (KD Scientific Legato 100, Illinois, USA), a glass syringe containing the polymer solution and connected to a stainless-steel blunt-ended needle. In order to concentrate the fibers on the multiscale hierarchical scaffold, the scaffold was placed in front of a flat aluminum collector plate (200 mm high and 50 mm wide) (figure S1(B)). To pre-strain the nanofibers of the sheath on the scaffold surface, the scaffold itself was maintained in a static position and intermittently put in rotation (approximately 20 rpm for 1 min every 5 min) while the sheath was being electrospun (figure 1(C)). The PLLA solution and the electrospinning parameters were the same as previously described.

2.3. Imaging: scanning electron microscopy (SEM) and high-resolution x-ray tomography

To examine the surface morphology of both PLLA single bundles and the multiscale hierarchical scaffolds, a SEM analysis was performed. A commercial SEM (Philips 515 SEM, Amsterdam, Netherlands) was used with an accelerating voltage of 15 kV, on samples sputter-coated with gold. The distribution of fiber diameters (mean and standard deviation) was measured on the SEM images of about 200 fibers, by means of an image analysis software ImageJ [35].

To investigate the three-dimensional structure of the PLLA single bundles, high-resolution x-ray tomographic scans were acquired with a high-resolution x-ray tomograph (Xradia 510 Versa, ZEISS, Pleasanton, CA, USA). For all the scans, the following settings were used: 40 kV Voltage, 3 W Power, 75.5 microAmpere tube current. Images were collected at rotational steps of 0.18° over 360°. Two different isotropic voxel sizes were obtained: (i) Voxel size 1 μm, using 8 s exposure time (scanning time of approximately 6 h); (ii) Voxel size 0.4 μm, using 14 s exposure time (scanning time of approximately 10 h).

To investigate the three-dimensional structure of the PLLA multiscale hierarchical scaffold, high-resolution x-ray tomographic scans were acquired with another high-resolution x-ray tomograph (Xradia 520 Versa, ZEISS, Pleasanton, CA, USA). The following parameters were used: 40 kV Voltage, 3 W Power, 75 microAmpere tube current. Two different isotropic voxel sizes were obtained: (i) 20 μm of voxel size to obtain a full view of the PLLA multiscale hierarchical scaffold for a length of 35 mm, by acquiring three consecutive scans, which were later assembled (this was obtained using 5 s exposure time, rotational steps of 0.22° over 360°, for a total scanning time of 9 h); and (ii) 8.5 μm of voxel size to visualize the internal PLLA single bundles and the sheath on a shorter portion (this was achieved with 7 s exposure time, rotational steps of 0.12° over 360°, for a scanning time of 7.5 h).

All the XCT images, were reconstructed using the Scout-and-Scan Reconstructor software (ZEISS), and were visualized using XM3DViewer1.2.8 software (ZEISS).

To measure the alignment of the nanofibers in the PLLA single bundles, the XCT scans at the highest resolution (0.4 μm of voxel size) were analyzed with the Directionality plugin of ImageJ [35–37]. The same procedure was applied to investigate the alignment of nanofibers and bundles inside the multiscale hierarchical scaffold, by using the Directionality plugin on the XCT scan of the multiscale scaffold with the highest resolution (8.5 μm of voxel size). This approach allowed the quantification of the number of nanofibers within a given angle from the axis of the specimens.

2.4. Mechanical characterization of the PLLA single bundles and multiscale hierarchical scaffolds

The mechanical properties of the PLLA single bundles and multiscale hierarchical scaffolds were measured with a monotonic tensile test to break using a servo-hydraulic testing machine (8032, Instron, High Wycombe, UK), with a ±1 kN dynamic cell (Instron,

High Wycombe, UK). The force signals had a noise of 0.01 N after filtering. All the specimens were immersed in saline for two minutes before the mechanical test.

To measure the diameter of each single bundle before the test, a polarized light optical microscope (Axioskop, ZEISS, Pleasanton, CA, USA) equipped with a camera (AxioCam MRc, ZEISS, Pleasanton, CA, USA) was used by means of an acquisition and image analysis software ImageJ [35]. For each PLLA single bundle, the mean and standard deviation of 10 measurements was computed.

Ten specimens of PLLA single bundles were tested. Dedicated capstan grips (figure 5(A)) were used to minimize the stress concentrations at sample ends. The gauge length was 47.42 mm (this included the free length and the portion of specimen wrapped around the capstans, consistently with the BS EN 12562:1999 and the ASTM D2256/D2256M-10 (2015) standards). The test machine was operated in displacement control, with an actuator speed of 16 mm s^{-1}, resulting in a strain rate of 33% s^{-1} (similar strain rates have been measured in tendons and ligaments while running [38]).

Five PLLA multiscale hierarchical scaffolds were subjected to a monotonic tensile test to break with a strain rate of 100% s^{-1} (similar strain rates have been measured in tendons during a run or rupture [39]). To measure the diameter of each PLLA multiscale hierarchical scaffold, six images were acquired (at three positions along the specimen, rotating the scaffold by 90°), and analyzed with ImageJ [35]. The diameter was measured ten times in each image. The diameter of each PLLA multiscale hierarchical scaffold was obtained as mean and standard deviation of 60 measurements. To minimize the stress concentrations, the extremities of the multiscale hierarchical scaffolds were potted in tapered stumps of acrylic cement. The stumps were fixed in the grips of the machine (figure 5(B)). As the length varied slightly between multiscale hierarchical scaffolds, in order to perform the test with the same strain rate of 100% s^{-1} (similar strain rates have been measured in tendons during a run or rupture [39]), the gauge length of each scaffold's specimen was measured with a caliper (mean and standard deviation of 5 measurements). The actuator rate was consequently adjusted for each specimen.

The following indicators were calculated as described in the supporting information (figure S2): Young Modulus (E), Yield Stress (σ_Y), Yield Strain (ε_Y), Failure Force (F_F), Failure Stress (σ_F), Failure Strain (ε_F), Work to Yield (L_Y), Work to Failure (L_F) (figure 5, supporting information tables S1–S3). After the test the gauge length of each single bundle and each multiscale hierarchical scaffold was weighed using a precision balance (MC 210 P, full scale 210 g, resolution 0.01 mg, Sartorius, Göttingen, Germany). The load-displacement curves were converted to stress–strain curves using two different approaches (figure 5):

- To describe the macroscopic mechanical behavior of the specimen, the apparent stress was computed dividing the force by the cross-sectional area measured before the test.
- To quantify the net mechanical properties, the net stress was also computed dividing the apparent stresses by the volume fraction (v) of the specimens.
- The apparent and the net Young Modulus (E), and unit works to failure were computed (L_Y, L_F)

The volume fraction (v) was calculated with the equation:

$$v = \frac{w}{(L \cdot A \cdot \rho)} \quad (1)$$

where:

w is the weight of the gauge length of the specimen.

L is length of the gauge length of the specimen.

A is the cross-sectional area of the specimen.

ρ is the density of the raw material (PLLA = 1.26 g cm^{-3}).

2.5. Cell testing

Human fibroblasts from a single donor, obtained from waste tissue under informed consent were kindly provided by Dr Vanessa Hearnden, University of Sheffield. They were maintained in α-MEM culture medium (Lonza®, UK), 10% foetal bovine serum (FBS, Labtech, UK), 2 mM L-glutamine (Sigma Aldrich, UK) and 100 mg ml^{-1} penicillin/streptomycin (Sigma Aldrich, UK). Fibroblasts were cultured at 37 °C in 5% CO_2 in a humidified incubator. The cells were passaged in 75 cm^2 tissue-culture flasks with media changes every 2–3 days. The cells were used between passage 4 and 6.

The PLLA multiscale hierarchical scaffolds were cut to 1 cm lengths and sterilized in 70 vol% ethanol for 1 h. Before seeding the PLLA multiscale hierarchical scaffolds were rinsed 3 times in phosphate buffered saline (PBS) (Sigma Aldrich, UK) to remove any remaining ethanol. The PLLA multiscale hierarchical scaffolds ($n = 9$) were seeded with 200 000 cells at a density of 1 000 000 cells ml^{-1} in a 24 well plate. The PLLA multiscale hierarchical scaffolds were seeded with half of the 200 000 cells on the top surface then immediately rotated and seeded with the remaining 100 000 cells on the bottom surface. The cells were left to attach to the scaffold for 45 min after which they were carefully submerged in 1 ml of media.

On days 1, 7, 14 and 16 a resazurin reduction (RR) assay was performed to measure the cell viability as previously described [40]. The scaffolds were transferred to new 24 well plates before the assay was performed to ensure only the viability of cells attached to the PLLA multiscale hierarchical scaffold was measured. 1 ml of resazurin salt solution (0.1 mM in α-MEM) was added to each well and incubated for 4 h. 200 μl of the reduced resazurin solution was

transferred into a 96 well plate and the fluorescence measured at 540 nm excitation and 630 nm emission using a spectrofluorometer (FLX800, BIO-TEK instruments Inc., Winooski, VT, USA). The PLLA multiscale hierarchical scaffolds were then washed twice in PBS before 1 μl of new media was added to the wells.

On day 14 of culture samples were fixed in 4 vol% formaldehyde for 30 min for histological analysis. The PLLA multiscale hierarchical scaffolds were placed in cassettes and ran through a tissue processor (Leica TP 1020, Wetzlar, GER), passing the samples though 70% industrial methylated spirits (IMS) for 1 h twice followed by a sequential dehydration at 80%, 85%, 90%, 95% and 100% twice for 1.5 h each. This was followed by clearing in Xylene twice for 1.5 h then infiltrating with paraffin wax for 2 h twice. The samples were then embedded in molten paraffin wax using an embedding center (Leica EG 1160, Wetzlar, Germany). The samples were then sectioned longitudinally at a thickness of 10 μm with a microtome (Leica RM2145, Wetzlar, Germany) and mounted onto glass slides. Following sectioning the samples were stained with haematoxylin and eosin.

2.6. Statistical analysis

The significance of differences between the apparent and net mechanical properties was assessed with a ratio paired parametric t-test both for the single bundles ($n = 10$), and for the multiscale hierarchical scaffolds ($n = 5$). The comparison between the single bundles and multiscale hierarchical scaffolds diameters, volume fractions and apparent and net mechanical properties were assessed with an unpaired parametric t-test with Welch's correction. The significant differences between the cell growth on the multiscale hierarchical scaffolds ($n = 9$) at the different time points was assessed with a one-way analysis of variance (ANOVA) followed (if $p \leqslant 0.05$) by the Tukey post-hoc test.

All statistical analyses were performed with Prism —GraphPad (GraphPad Software, San Diego, CA, USA).

3. Results and discussion

3.1. Production process of the PLLA multiscale hierarchical scaffold

In order to reproduce the complex hierarchical structure of the tendons and ligaments [4, 5] (figure 1(A)), we first produced PLLA single bundles mimicking natural collagen fascicles, by means of electrospinning on a high-speed rotating drum collector (figure S1(A)). This process allowed production of bundles of aligned nanofibers of PLLA, similar to the fascicles composing tendons and ligaments [4–6] (figure 1(B)). To produce a scaffold with a relevant thickness (e.g. comparable to the antero-posterior thickness of the human Achilles tendon [41] or to the diameter of the anterior cruciate ligament [42]), we prepared groups of 100 bundles each with a length of 100 mm, aligned to each other and fixed at the extremities (figure S1(B)). To replicate the membrane wrapping the tendons and ligaments (respectively named epitenon and epiligament [4]), a non-aligned nanofibrous sheath was electrospun onto the group of bundles (figure 1(C)). Alternating rotations and stops while electrospinning the sheath allowed the nanofibers to stretch and wrap around the group of bundles. As a result, the overall diameter of the scaffold was reduced, thus allowing to compact more bundles in the same cross-section, and enhance the mechanical strength.

The final multiscale hierarchical scaffold had similar macroscopic dimensions, but also micro- and nano-structure and hierarchical organization similar to natural tendons and ligaments (figure 1(D)).

3.2. Morphology of the PLLA single bundles and multiscale hierarchical scaffold

In order to assess the morphology of the nanofibers, of the single bundles and of the entire PLLA multiscale hierarchical scaffold, we performed a SEM (figure 2). The SEM investigation showed that the nanofibers of the PLLA single bundles and the sheaths were homogeneous, smooth, continuous and produced without bead defects. The nanofibers in the bundles showed a preferential direction, as desired to replicate the arrangement of the fibrils in the tendons and ligaments [43]. Conversely the nanofibers in the sheath were randomly arranged, similar to the natural epitenon and epiligament [4]. The nanofibers forming the single bundles and the sheath had similar diameters of 0.59 ± 0.14 μm (figures 2(D)–(F)). The single bundles had diameters of 586.5 ± 38.0 μm (figure 2(C)). The PLLA multiscale hierarchical scaffolds, had a mean diameter of 6.5 ± 0.8 mm (figures 2(A) and (B)). These dimensions are comparable to those found in the hierarchical organization of the fibrils and fascicles in the tendons and ligaments [4, 5, 41, 42].

To investigate the arrangement of the nanofibers of the PLLA single bundles and of the multiscale hierarchical scaffold in the entire volume, we performed a high-resolution x-ray tomography (XCT) investigation (figure 3). This technique has only recently become available at sub-micrometer resolution; it is extremely difficult to implement in on low-density materials such as the electrospun polymer fibers [16, 22, 44, 45].

Analyzing the multiscale hierarchical scaffolds with the XCT, we were able to confirm that all the bundles were tightly placed side by side, and were aligned along

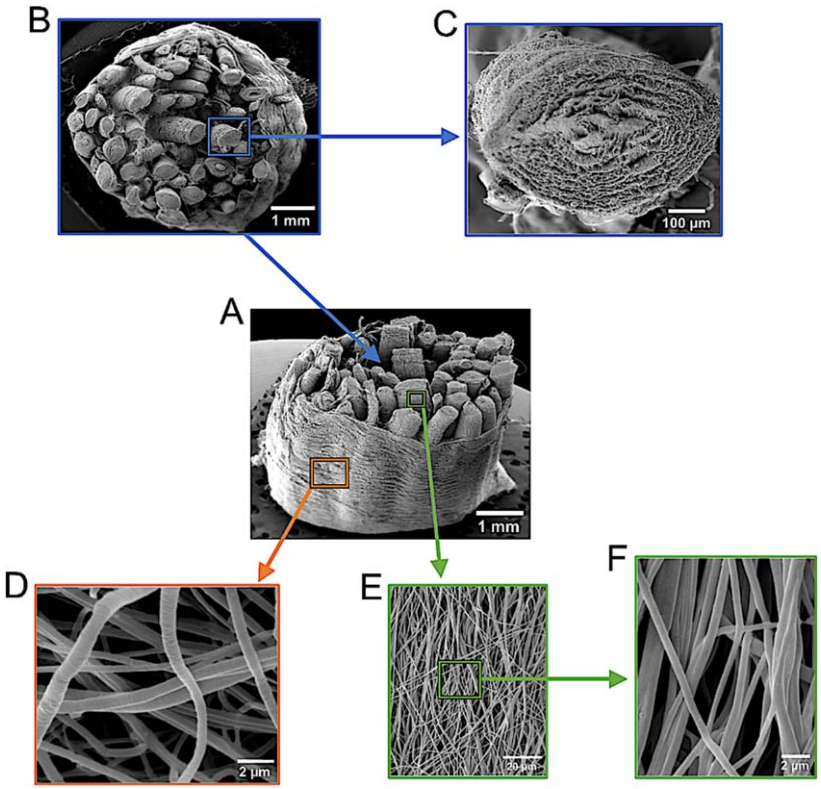

Figure 2. SEM images of the PLLA multiscale hierarchical scaffold. (A), (B) Section of the multiscale hierarchical scaffold made of single bundles of aligned nanofibers with the electrospun sheath epitenon/epiligament-like. (C) Section of a single bundle. (E), (F) Aligned nanofibers on the surface of a single bundle at different magnifications. (G) PLLA nanofibers of the sheath.

the axis of the scaffold (figure 3 and supplementary information Movies S1–S4). The Directionality analysis confirmed a preferential axial alignment of the nanofibers with a Gaussian-like dispersion (figure 4). Inside the single bundles 51.5% of the nanofibers lay within 15° from the axis of the bundle, while fewer than 7% were between 75° and 90° from the axis. In the multiscale hierarchical scaffolds, 51.6% of nanofibers were oriented in a range of 0°–3° while 6.1% of nanofibers were oriented in the range of 75°–90°. This alignment resembles the natural alignment of collagen in tendons and ligaments [43]. The external sheath was visible in the XCT, it completely wrapped the multiscale hierarchical scaffold, and showed a porous structure.

3.3. Mechanical properties of the PLLA single bundles and of the multiscale hierarchical scaffold

To measure the mechanical properties of the single bundles and of the multiscale hierarchical scaffold, we performed tensile testing (figure 5 and supporting information tables S1–S4). To minimize stress concentrations at the extremities we designed a dedicated test including specific capstan fixtures for the single bundles and potted extremities for the multiscale hierarchical scaffolds.

Both the single bundles and the multiscale hierarchical scaffolds showed a nonlinear toe region up to 2%–5% strain, similar to the nonlinear behavior of natural fascicles of tendons and ligaments [3–5]. After the toe region, both the single bundles and the multiscale hierarchical scaffolds exhibited a linear elastic behavior (again, similar to the behavior of the natural tendons and ligaments). The apparent modulus of elasticity was 156.2 ± 36.7 MPa for the single bundles, and 116.9 ± 19.7 MPa for the multiscale hierarchical scaffolds. The single bundles began to yield at an apparent stress of 15.8 ± 2.8 MPa, while the multiscale hierarchical scaffolds at 6.2 ± 0.9 MPa. It must be noted that the change of slope identified as yield (consistently with the guidelines for material testing, see supporting information (figure S2)) is partly due to a proper yield of the material, and partly to the failure of individual nanofibers. These phenomena could not be separated in our tensile test.

After yield, both the single bundles and the multiscale hierarchical scaffolds exhibited a ductile behavior, reaching high strain (up to 30%) before failing. This provides a wide safety factor in case of partial damage, before catastrophic failure occurs. In fact, high energy was required to induce failure in both the PLLA single bundles and the multiscale hierarchical scaffolds (supplementary information tables S1–S3). Final failure of the single bundles occurred at an apparent failure stress of 18.5 ± 3.3 MPa and of the multiscale hierarchical scaffolds at 7.7 ± 1.4 MPa.

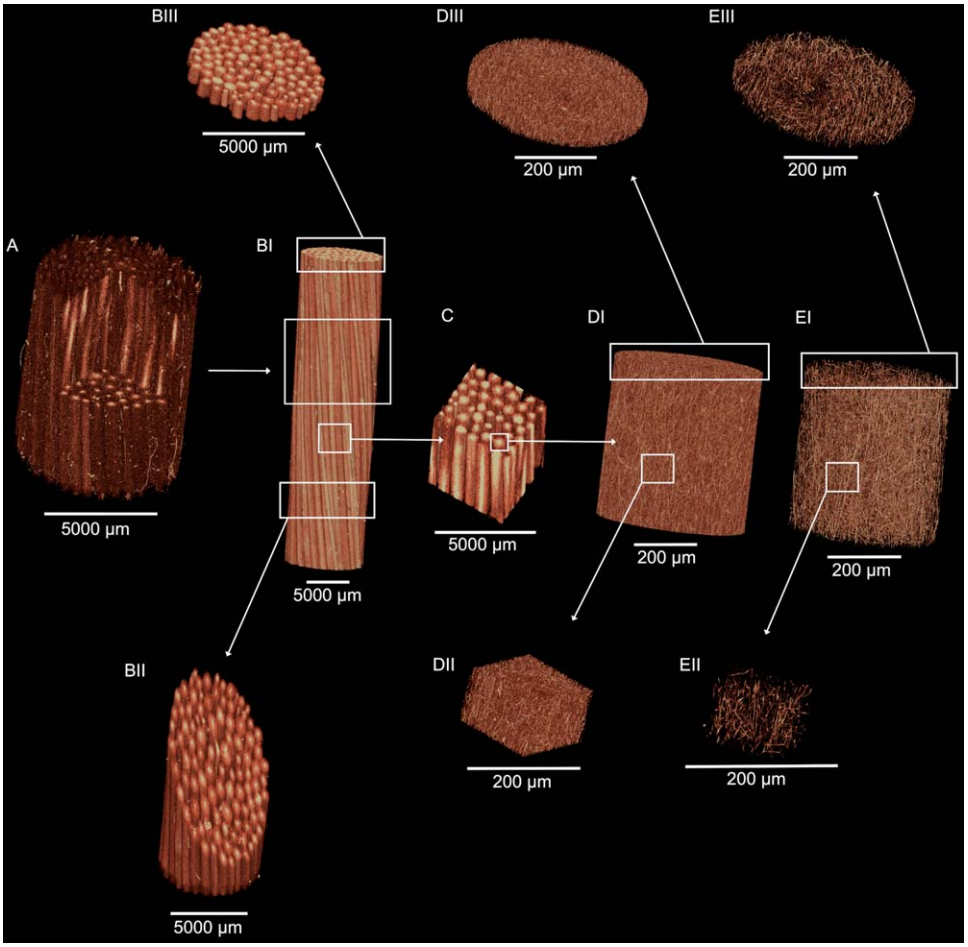

Figure 3. High-resolution x-ray tomographic images of the hierarchical structure of the PLLA multiscale hierarchical scaffold. (A) section of a multiscale hierarchical scaffold in which the nanofibrous sheath and the internal single bundles are visible (voxel size: 8.5 μm). (BI) Overview of a multiscale hierarchical scaffold in which the axially aligned single bundles are visible (voxel size: 20 μm). (BII, BIII) Crop of the multiscale hierarchical scaffolds showing a section of the internal single bundles (voxel size: 20 μm). (C) Crop of the internal part of the multiscale hierarchical scaffold with the single axially aligned bundles (voxel size: 20 μm). (DI) section of a PLLA single bundle of axially aligned nanofibers (voxel size: 0.4 μm). (DII) Cubic crop of the single bundle showing also all the internal nanofibers axially aligned across the section (voxel size: 0.4 μm). (DIII) Circular slice of the single bundle with all the nanofibers (voxel size 0.4 μm). (EI, EII, EIII) By tuning the thresholding it is possible to display just the internal nanofibers of the single bundle (voxel size: 0.4 μm).

For the PLLA single bundles, the stiffness was comparable to those of the fascicles of natural tendon (range: 40–400 MPa [5, 46]) and ligament (range: 320–345 MPa [47]). The maximum apparent stress of the PLLA single bundles was also comparable to the fascicles of natural tendons (range: 6–40 MPa [5, 46]) and ligaments (range: 34–36 MPa [47]). The maximum deformation of the single bundles exceeded that of fascicles of natural tendon (range: 9–25 MPa [5, 46]) and ligament (range: 14–15 MPa [47]). Therefore, the energy absorbed before failure of the PLLA single bundles (i.e. the apparent work to failure) was also greater than for the natural fascicles. The multiscale hierarchical scaffold exhibited a similar apparent stiffness to natural tendon (range: 65–3000 MPa [5, 48]) and ligament (range: 20–700 MPa [5, 48]). The apparent yield stress and failure stress of the multiscale hierarchical scaffold was lower that of natural tendon (range: 20–116 MPa [5, 48]) and ligament (range: 1–46 MPa [5, 48]). The maximum deformation of the multiscale hierarchical scaffolds was in the same range of the natural tendons (range: 14–59 MPa [5, 48]) and ligaments (range: 8–120 MPa [5, 48]). Considering the planned applications in reconstructive surgery, it is important that the multiscale scaffold has lower strength than natural tendons and ligaments; to avoid damage in the patient's repaired site in a case of overload, failure should initiate in the implanted device, rather than in the host tissue.

As expected, the apparent modulus of elasticity and the apparent yield and failure stress in the multiscale scaffold was lower than for the single bundles. This has a simple explanation: the stress in the multiscale scaffold is calculated over the total cross-sectional area (which

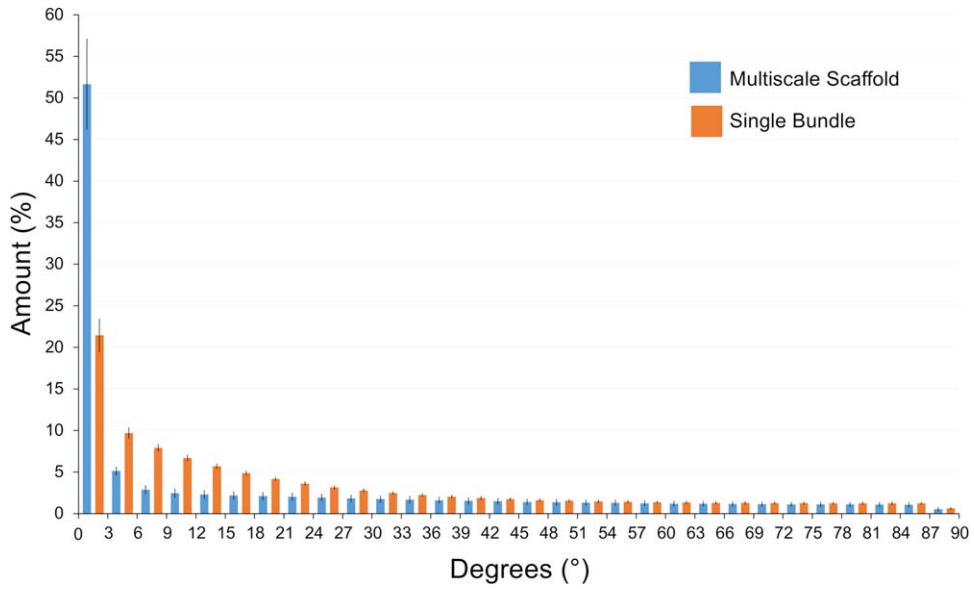

Figure 4. Directionality analysis on the single bundle and the multiscale hierarchical scaffold. An angle of 0° means that the nanofibers were aligned with the longitudinal axis of the specimens, an angle of 90° means that nanofibers were perpendicular to the longitudinal axis of the specimens.

includes the actual cross section of the bundles, but also some unavoidable empty space).

In fact, for the single bundles the net Young modulus, yield stress, failure stress, work to yield and failure (i.e. scaled according to the volume fraction) were 4.4–4.6 times larger than the apparent ones (ratio paired t-test, $p \leqslant 0.0001$, figure 5 and supporting information tables S1 and S2). The net mechanical properties of the multiscale hierarchical scaffolds were 6.1–6.3 times larger than the apparent ones (ratio paired t-test, $p \leqslant 0.0001$).

Furthermore, the system used for clamping the extremities of the multiscale scaffold caused some stress concentration (in fact the scaffolds started failing at the one of the extremities) whereas loading on the single bundles prevented such artifact (in fact all the single bundles failed in the central portion of the specimen). The strain rates we adopted (33% s^{-1} for the single bundles and 100% s^{-1} for the multiscale hierarchical scaffolds) are in the range of those experienced by tendons and ligaments during strenuous physiological activities [38, 39, 49–52]. It must be noted that the tests performed so far were monotonic. Fatigue tests might offer further insight about the mechanical strength of the scaffolds under cyclic loading.

In the destructive tests on the multiscale scaffolds the external sheath contained and kept together the bundles after the individual ones began to fail. This effect provided better structural behavior of the scaffold. Most previous scaffolds for tendon and ligament replacements consist of braided, twisted or knitted fibers [23, 27–30], which do not replicate the morphology of natural tissue. Our approach allowed a compaction of the single bundles inside the multiscale hierarchical scaffold, while maintaining a biomimetic hierarchical structure. In fact, although assembling multiple bundles (with a circular cross-section) unavoidably leaves some empty space between them, the volume fraction of the hierarchical scaffold was only 24% lower in the hierarchical assembly (supporting information table S3), thanks to tight wrapping of the external sheath.

In the past, Banik *et al* produced a tendon-inspired scaffold, with a custom-made gap-collector: this allowed the alignment of the nanofibers between the two cylindrical collectors but without any possibility to compact them [27]. To achieve some compaction, Bosworth and Mouthuy *et al* braided or twisted together multiple bundles or yarns of their tendon scaffolds [23, 29]. More recently Laranjeira *et al* applied different textile techniques, to join together several groups of bundles twisted together, obtaining braided and flat scaffolds [30]. However, these textile arrangements lost a biomimetic structure, not allowing a combination of compaction and axial alignment of their substructures. Not surprisingly, most of the scaffolds developed in the past focused on the regeneration of peripheral nerves, where mechanical strength is not essential. For example, Li *et al* produced scaffolds for nerve regeneration, by fixing several bundles along the axis of a drum collector, and finally covering them with an electrospun sheath. Removing the drum increased the free space inside the scaffolds [34].

3.4. Cell growth

To evaluate the suitability of the PLLA multiscale hierarchical scaffolds for cell culture, resazurin

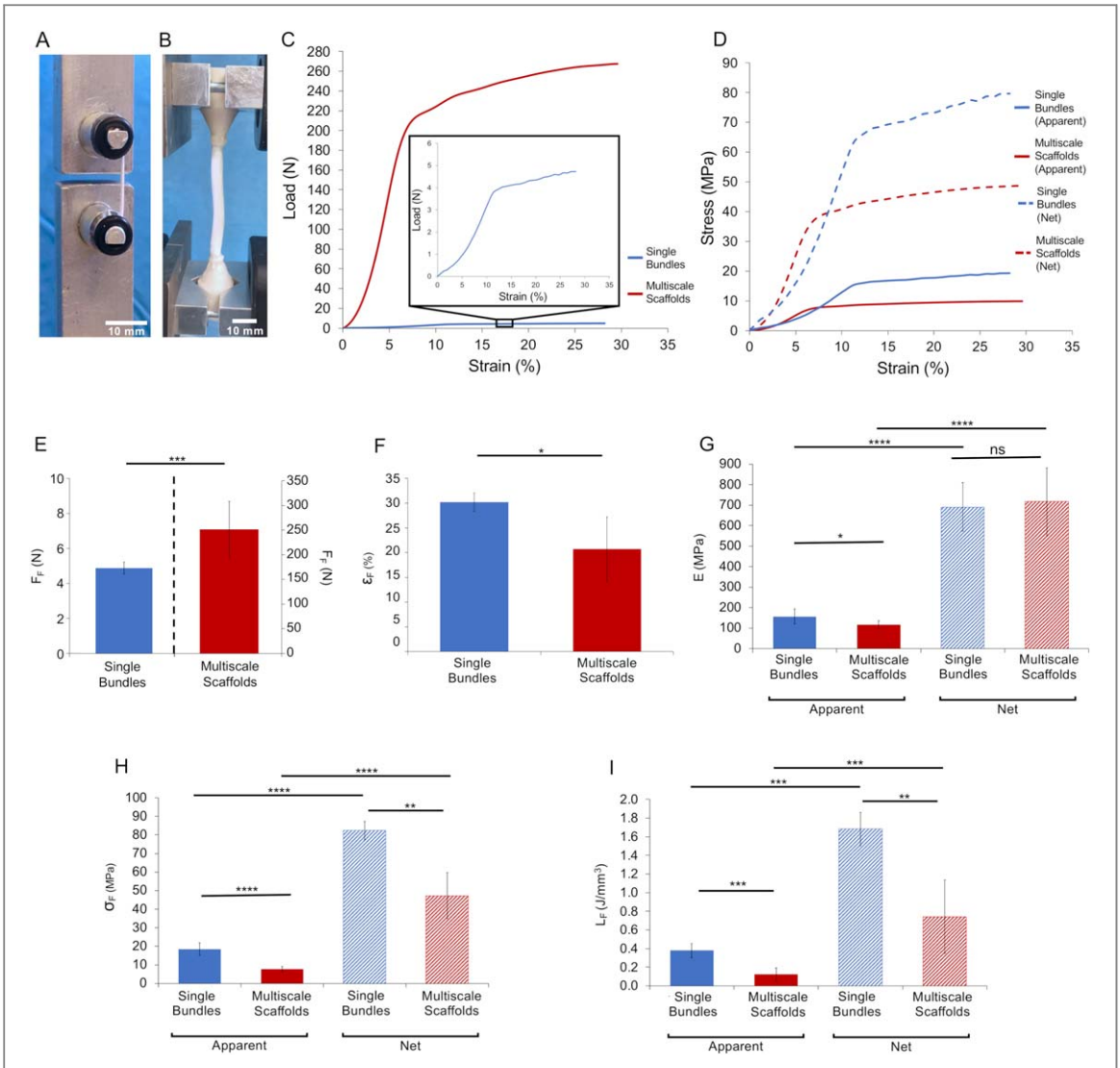

Figure 5. Mechanical tensile testing of the PLLA single bundles and multiscale hierarchical scaffolds. (A) Capstan grips for the single bundles. (B) Setup for the multiscale hierarchical scaffolds. (C) Example of load-strain curves of a typical single bundle and a typical multiscale hierarchical scaffold (square box: zoom-in of the single bundle curve). (D) Example of the apparent (solid lines) and net (dashed lines) stress–strain curves of a single bundle and a multiscale hierarchical scaffold. Comparison of the mechanical properties between single bundles and multiscale hierarchical scaffolds: (E) failure force (F_F) (left axis refers to the single bundles, right axis to the multiscale hierarchical scaffolds); (F) failure strain (ε_F) (G) Young Modulus (apparent = solid bars; net = dashed bars); (H) failure stress (σ_F) (apparent = solid bars; net = dashed bars) and (I) work to failure (L_F) (apparent = solid bars; net = dashed bars). The mean and standard deviation are represented for each group. The statistical significance of differences is indicated ($^{*}p \leqslant 0.05$, $^{**}p \leqslant 0.01$, $^{***}p \leqslant 0.001$, $^{****}p < 0.0001$, ns = not significant).

reduction assays were performed on days 1, 7, 14 and 16 (figure 6). The multiscale hierarchical scaffolds showed an increase in the number of cells indicated by the increase in cell metabolic activity between day 1 and 16, suggesting an increase in the number of cells present on the scaffolds by day 16. The difference of fluorescence values between the day 1–14 and 1–16 was statistically significant (one-way ANOVA $p \leqslant 0.05$).

To assess the cells spatial distribution and morphology within the multiscale hierarchical scaffolds, histological sectioning with haematoxylin and eosin staining was performed (figure 6). Sections were analyzed at the seeded surfaces, the side 'walls' and the core of the multiscale hierarchical scaffolds. Cells were present in all regions of the multiscale hierarchical scaffold, suggesting cells were capable of penetrating into the interior region of the scaffold from the upper and lower seeded surfaces. Cells can be seen growing into the fibers of the multiscale hierarchical scaffolds in the sections taken from the side of the scaffolds. The porous sheath of nanofibers also allowed cell migration inside the scaffold. Within the core of the multiscale hierarchical scaffold cells were densely packed between the individual fibers of the scaffold, similar to the cellular arrangement within the interfascicular matrix of native tendons and ligaments, which has been shown to play an important role in the sliding mechanisms of tendons and ligaments [53–55].

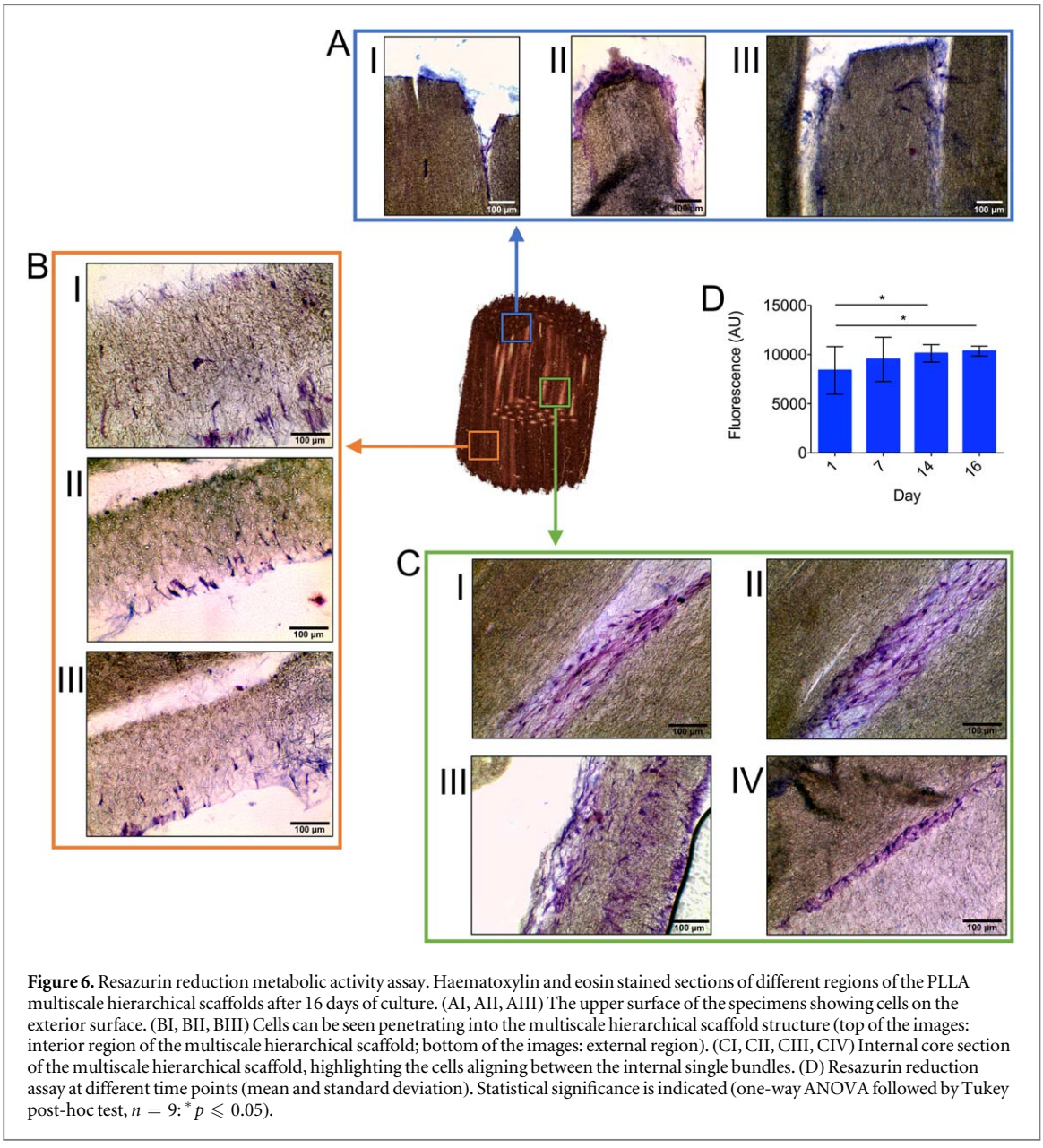

Figure 6. Resazurin reduction metabolic activity assay. Haematoxylin and eosin stained sections of different regions of the PLLA multiscale hierarchical scaffolds after 16 days of culture. (AI, AII, AIII) The upper surface of the specimens showing cells on the exterior surface. (BI, BII, BIII) Cells can be seen penetrating into the multiscale hierarchical scaffold structure (top of the images: interior region of the multiscale hierarchical scaffold; bottom of the images: external region). (CI, CII, CIII, CIV) Internal core section of the multiscale hierarchical scaffold, highlighting the cells aligning between the internal single bundles. (D) Resazurin reduction assay at different time points (mean and standard deviation). Statistical significance is indicated (one-way ANOVA followed by Tukey post-hoc test, $n = 9$: $^{*}p \leqslant 0.05$).

4. Conclusion

We have developed an innovative method to produce a scaffold for the repair and regeneration of tendons and ligaments. We used high-resolution x-ray tomography to investigate the morphology of the PLLA single bundles and of the multiscale hierarchical scaffold, from nano- to micrometric resolution. Our hierarchical approach allowed mimicking of the multiscale arrangement of the collagen fibrils and fascicles in the ligaments and tendons. Moreover, the developed scaffold provided comparable stiffness to the natural tendons and ligaments. As required by safety criteria for implantable materials and devices, the strength of our multiscale scaffold (7.7 ±1.4 MPa) was lower than that of the natural tissues where it would be hosted (1–46 MPa for the ligaments, and 20–116 MPa for tendons). We demonstrated that the porous sheath of nanofibers allowed cell growth and migration in the interior of the scaffold after 14 d of cell culture in static conditions, thus providing an ideal environment for cell proliferation. While so far we focused on pure PLLA constructs, this technological platform can be applied to a broad spectrum of synthetic and natural polymers to customize scaffold properties for specific patients and applications.

Acknowledgments

FP7 COST Action MP1206 'Electrospun Nano-fibers for bio inspired composite materials and innovative industrial applications' and the Italian Ministry of University and Research (MIUR) are acknowledged. Carlo Gotti, Elisa Bendanti and Rachna Parwani are acknowledged for their help in the specimens' preparation, mechanical characterization and technical

support in the XCT image acquisition respectively. The ZEISS Global Centre at the School of Engineering (University of Portsmouth) is acknowledged for providing XCT facilities. The mobility of Alberto Sensini was funded by university of Bologna (Marco Polo grant). LB was supported by an Engineering and Physical Sciences (EPSRC) UK doctoral training grant: EP/M506618/1.

ORCID iDs

Chiara Gualandi https://orcid.org/0000-0002-2020-1892
Maria Letizia Focarete https://orcid.org/0000-0003-0681-5887
Andrea Zucchelli https://orcid.org/0000-0002-3466-2913
Liam Boyle https://orcid.org/0000-0003-4122-7941
Gwendolen C Reilly https://orcid.org/0000-0003-1456-1071
Alexander P Kao https://orcid.org/0000-0001-5376-1661
Gianluca Tozzi https://orcid.org/0000-0002-3172-5720
Luca Cristofolini https://orcid.org/0000-0002-7473-6868

References

[1] Liu C-F, Aschbacher-Smith L, Barthelery N J, Dyment N, Butler D and Wylie C 2011 What we should know before using tissue engineering techniques to repair injured tendons: a developmental biology perspective *Tissue Eng.* B **17** 165–76
[2] Rees J D, Wilson A M and Wolman R L 2006 Current concepts in the management of tendon disorders *Rheumatology* **45** 508–21
[3] Woo S L Y, Abramowitch S D, Kilger R and Liang R 2006 Biomechanics of knee ligaments: injury, healing, and repair *J. Biomech.* **39** 1–20
[4] Kannus P 2000 Structure of the tendon connective tissue *Scand. J. Med. Sci. Sport.* **10** 312–20
[5] Goh K L, Listrat A and Béchet D 2014 Hierarchical mechanics of connective tissues: integrating insights from nano to macroscopic studies *J. Biomed. Nanotechnol.* **10** 2464–507
[6] Hampson K, Forsyth N R, El Haj A and Maffulli N 2008 Tendon Tissue Engineering *Topics in Tissue Engineering* (4) ed N Ashammakhi *et al* vol 4 (Oulu, Finland: Expertissues) ch 3 pp 1–21 https://oulu.fi/spareparts/ebook_topics_in_t_e_vol4/abstracts/hampson.pdf
[7] James S L, Bates B T, Osternig L R and Oregon E 1978 Injuries to runners *Am. J. Sports Med.* **6** 40–50
[8] Dy C J, Daluiski A, Do H, Hernandez-Soria A, Marx R and Lyman S 2012 The epidemiology of reoperation after flexor tendon repair *J. Hand Surg. Am.* **37A** 919–24
[9] Lomas A J *et al* 2015 The past, present and future in scaffold-based tendon treatments *Adv. Drug Deliv. Rev.* **84** 257–77
[10] Sharma P and Maffulli N 2005 Tendon injury and tendinopathy: healing and repair *J. Bone Jt. Surg.* **87** 187–202
[11] Verdiyeva G, Koshy K, Glibbery N, Mann H and Seifalian A M 2015 Tendon reconstruction with tissue engineering approach —a review *J. Biomed. Nanotechnol.* **11** 1495–523
[12] Liu Y, Ramanath H S and Wang D A 2008 Tendon tissue engineering using scaffold enhancing strategies *Trends Biotechnol.* **26** 201–9
[13] Mo X, Wu T, Sun B and El-Hamshary H 2017 Nanofiber composites in tendon tissue engineering *Nanofiber Composites for Biomedical Applications* ed M Ramalingam and S Ramakrishna (Amsterdam: Elsevier) ch 14 345–67
[14] Sensini A and Cristofolini L 2018 Biofabrication of electrospun scaffolds for the regeneration of tendons and ligaments *Materials* **11** 1963
[15] Sensini A, Gualandi C, Cristofolini L, Tozzi G, Dicarlo M, Teti G, Belmonte-Mattioli M and Focarete M L 2017 Biofabrication of bundles of poly (lactic acid) -collagen blends mimicking the fascicles of the human Achille tendon *Biofabrication* **9** 1–13
[16] Sensini A, Cristofolini L, Focarete M L, Belcari J, Zucchelli A, Kao A and Tozzi G 2018 High-resolution x-ray tomographic morphological characterisation of electrospun nanofibrous bundles for tendon and ligament regeneration and replacement *J. Microsc.* **272** 196–206
[17] Pedde R D *et al* 2017 Emerging biofabrication strategies for engineering complex tissue constructs *Adv. Mater.* **29** 1–27
[18] Santos M L, Rodrigues M T, Domingues R M A, Reis R L and Gomes M E 2017 Biomaterials as Tendon and Ligament Substitutes: Current Developments *Regenerative Strategies for the Treatment of Knee Joint Disabilities* (*Studies in Mechanobiology, Tissue Engineering and Biomaterials*) ed J M Oliveira and R L Ruis vol 21 (Switzerland: Springer) ch 17 pp 349–71
[19] Ali U, Zhou Y, Wang X and Lin T 2011 Electrospinning of continuous nanofiber bundles and twisted nanofiber yarns *Nanofibers—Prod. Prop. Funct. Appl.* ed Tong Lin Dr. (Croatia: InTech) ch 8 153–74
[20] O'Connor R A and McGuinness G B 2016 Electrospun nanofibre bundles and yarns for tissue engineering applications: a review *Proc. Inst. Mech. Eng.* H **230** 987–98
[21] Bosworth L A, Alam N, Wong J K and Downes S 2013 Investigation of 2D and 3D electrospun scaffolds intended for tendon repair *J. Mater. Sci., Mater. Med.* **24** 1605–14
[22] Bosworth L A, Rathbone S R, Bradley R S and Cartmell S H 2014 Dynamic loading of electrospun yarns guides mesenchymal stem cells towards a tendon lineage *J. Mech. Behav. Biomed. Mater.* **39** 175–83
[23] Bosworth L A 2014 Travelling along the clinical roadmap: developing electrospun scaffolds for tendon repair *Conf. Pap. Sci.* **2014** 1–6
[24] Xu Y *et al* 2013 Fabrication of electrospun poly(L-Lactide-co-ε-Caprolactone)/collagen nanoyarn network as a novel, three-dimensional, macroporous, aligned scaffold for tendon tissue engineering *Tissue Eng.* C **19** 925–36
[25] Pauly H M, Kelly D J, Popat K C, Trujillo N A, Dunne N J, McCarthy H O and Haut Donahue T L 2016 Mechanical properties and cellular response of novel electrospun nanofibers for ligament tissue engineering: effects of orientation and geometry *J. Mech. Behav. Biomed. Mater.* **61** 258–70
[26] Sensini A, Gualandi C, Zucchelli A, Boyle L, Kao A P, Reilly G C, Tozzi G, Cristofolini L and Focarete M L 2018 Tendon fascicle-inspired nanofibrous scaffold of polylactic acid/collagen with enhanced 3d-structure and biomechanical properties *Sci. Rep.* **8** 1–15
[27] Banik B L, Lewis G S and Brown J L 2016 Multiscale poly-(ε-caprolactone) scaffold mimicking non-linearity in tendon tissue mechanics *Regen. Eng. Transl. Med.* **2** 1–9
[28] Xu Y *et al* 2014 The effect of mechanical stimulation on the maturation of TDSCs-poly(L-lactide-co-e-caprolactone)/collagen scaffold constructs for tendon tissue engineering *Biomaterials* **35** 2760–72
[29] Mouthuy P-A, Zargar N, Hakimi O, Lostis E and Carr A 2015 Fabrication of continuous electrospun filaments with potential for use as medical fibres *Biofabrication* **7** 25006
[30] Laranjeira M, Domingues R M A, Costa-Almeida R, Reis R L and Gomes M E 2017 3D mimicry of native-tissue-fiber architecture guides tendon-derived cells and adipose stem cells into artificial tendon constructs *Small* **13** 1–13

[31] Zhou F L, Gong R-H and Porat I 2010 Nano-coated hybrid yarns using electrospinning *Surf. Coatings Technol.* **204** 3459–63
[32] Naghashzargar E, Farè S, Catto V, Bertoldi S, Semnani D, Karbasi S and Tanzi M C 2015 Nano/micro hybrid scaffold of PCL or P3HB nanofibers combined with silk fibroin for tendon and ligament tissue engineering *J. Appl. Biomater. Funct. Mater.* **13** e156–68
[33] Padmakumar S, Joseph J, Neppalli M H, Mathew S E, Nair S V, Shankarappa S A and Menon D 2016 Electrospun polymeric core-sheath yarns as drug eluting surgical sutures *ACS Appl. Mater. Interfaces* **8** 6925–34
[34] Li D, Pan X, Sun B, Wu T, Chen W, Huang C, Ke Q, EI-Hamshary H A, Al-Deyab S S and Mo X 2015 Nerve conduits constructed by electrospun P(LLA-CL) nanofibers and PLLA nanofiber yarns *J. Mater. Chem.* B **3** 8823–31
[35] Liu Z 1991 Scale space approach to directional analysis of images *Appl. Opt.* **30** 1369–73
[36] Schindelin J *et al* 2012 Fiji: an open-source platform for biological-image analysis *Nat. Methods* **9** 676–82
[37] Schneider C A, Rasband W S and Eliceiri K W 2012 NIH Image to ImageJ: 25 years of image analysis *Nat. Methods* **9** 671–5
[38] Peltonen J, Cronin N J, Stenroth L, Finni T and Avela J 2013 Viscoelastic properties of the achilles tendon *in vivo* *Springerplus* **2** 1–8
[39] Lyght M, Nockerts M, Kernozek T W and Ragan R 2016 Effects of foot strike and step frequency on Achilles tendon stress during running *J. Appl. Biomech.* **32** 365–72
[40] O'Brien J, Wilson I, Orton T and Pognan F 2000 Investigation of the Alamar Blue (resazurin) fluorescent dye for the assessment of mammalian cell cytotoxicity *Eur. J. Biochem.* **267** 5421–6
[41] Pang B S and Ying M 2006 Sonographic measurement of Achilles tendons in asymptomatic subjects *J. Ultrasound Med.* **25** 1291–6
[42] Triantafyllidi E, Paschos N K, Goussia A, Barkoula N M, Exarchos D A, Matikas T E, Malamou-Mitsi V and Georgoulis A D 2013 The shape and the thickness of the anterior cruciate ligament along its length in relation to the posterior cruciate ligament: a cadaveric study *Arthrosc.—J. Arthrosc. Relat. Surg.* **29** 1963–73
[43] Radaelli F, D'Alfonso L, Collini M, Mingozzi F, Marongiu L, Granucci F, Zanoni I, Chirico G and Sironi L 2017 μMAPPS: a novel phasor approach to second harmonic analysis for *in vitro -in vivo* investigation of collagen microstructure *Sci. Rep.* **7** 17468
[44] Bradley R S, Robinson I K and Yusuf M 2017 3D X-ray nanotomography of cells grown on electrospun scaffolds *Macromol. Biosci.* **17** 1–8
[45] Maksimcuka J, Obata A, Sampson W W, Blanc R, Gao C, Withers P J, Tsigkou O, Kasuga T, Lee P D and Poologasundarampillai G 2017 X-ray tomographic imaging of tensile deformation modes of electrospun biodegradable polyester fibers *Front. Mater.* **4** 1–11
[46] Hanson P, Aagaard P and Magnusson S P 2012 Biomechanical properties of isolated fascicles of the Iliopsoas and Achilles tendons in African American and Caucasian men *Ann. Anat.* **194** 457–60
[47] Butler D L, Kay M D and Stouffer D C 1986 Fascicle-bone units from human patellar tendon and knee ligaments *J. Biomech.* **19** 425–32
[48] Connie S, Vanderby C J and Vanderby R J 2016 Ligament and Tendon *Handbook of Biomaterial Properties* ed W Murphy, J Black and G Hastings (New York: Springer) ch B3 55–62
[49] Butler D L 1989 Anterior cruciate ligament: its normal response and replacement *J. Orthop. Res.* **7** 910–21
[50] Lewis G and Shaw K M 1997 Tensile properties of human tendo Achillis: effect of donor age and strain rate *J. Foot Ankle Surg.* **36** 435–45
[51] Wren T A, Yerby S A, Beaupré G S and Carter D R 2001 Mechanical properties of the human achilles tendon *Clin. Biomech.* **16** 245–51
[52] Lee M and Hyman W 2002 Modeling of failure mode in knee ligaments depending on the strain rate *BMC Musculoskelet. Disord.* **3** 1–8
[53] Spiesz E M, Thorpe C T, Chaudhry S, Riley G P, Birch H L, Clegg P D and Screen H R C 2015 Tendon extracellular matrix damage, degradation and inflammation in response to *in vitro* overload exercise *J. Orthop. Res.* **33** 889–97
[54] Spiesz E M, Thorpe C T, Thurner P J and Screen H R C 2018 Structure and collagen crimp patterns of functionally distinct equine tendons, revealed by quantitative polarised light microscopy (qPLM) *Acta Biomater.* **70** 281–92
[55] Thorpe C T and Screen H R C 2016 Tendon Structure and Composition *Metabolic Influences on Risk for Tendon Disorders* (*Advances in Experimental Medicine and Biology*) ed P W Ackermann and D A Hart vol 920 (Berlin: Springer) ch 1 pp 3–10